Supporting Information

Field-Effect Tuned Adsorption-Dynamics of VSe_2 Nanosheets for Enhanced Hydrogen Evolution Reaction

Mengyu Yan [†,‡], Xuelei Pan[†], Peiyao Wang[§], Fei Chen[†], Liang He[†], Gengping Jiang[‖,§] , Junhui Wang[†], Jefferson Z. Liu[§], Xu Xu[†,], Xiaobin Liao[†], Jihui Yang[‡] & Liqiang Mai[†,*]*

[†]State Key Laboratory of Advanced Technology for Materials Synthesis and Processing, Wuhan University of Technology, Wuhan 430070, China,

[‡]Materials Science and Engineering Department, University of Washington, Seattle, Washington 98195-2120, United States

[§]Department of Mechanical and Aerospace Engineering, Monash University, Victoria 3800, Australia

[‖]College of Science, Wuhan University of Science and Technology, Wuhan 430081, China

Corresponding Author:

mlq518@whut.edu.cn (L. M.)

xuxu@whut.edu.cn (X. X.)

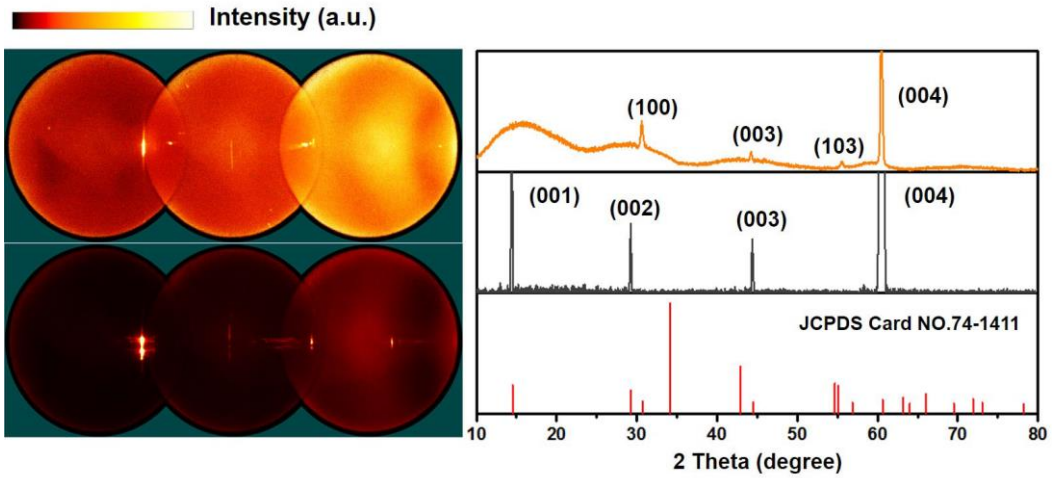

Figure S1. The 2D X-ray diffraction spectra and the corresponding pattern. The orange spectrum is the XRD results of the VSe_2 sample after mechanical exfoliation. The gray spectrum is measured from bulk VSe_2 (single crystal). The data of exfoliated VSe_2 sample is collected with the support of the tape which is used for exfoliation.

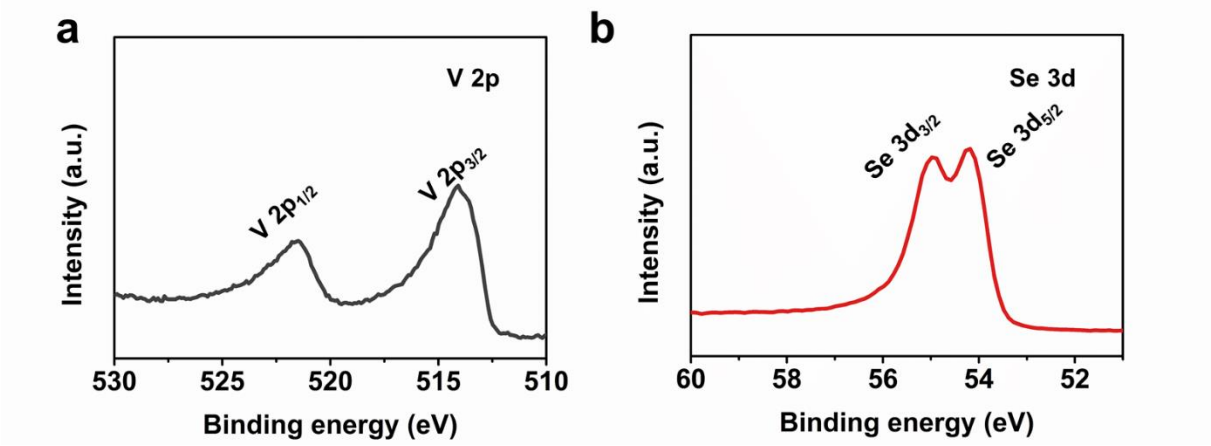

Figure S2. High-resolution XPS spectra of V (a) and Se (b).

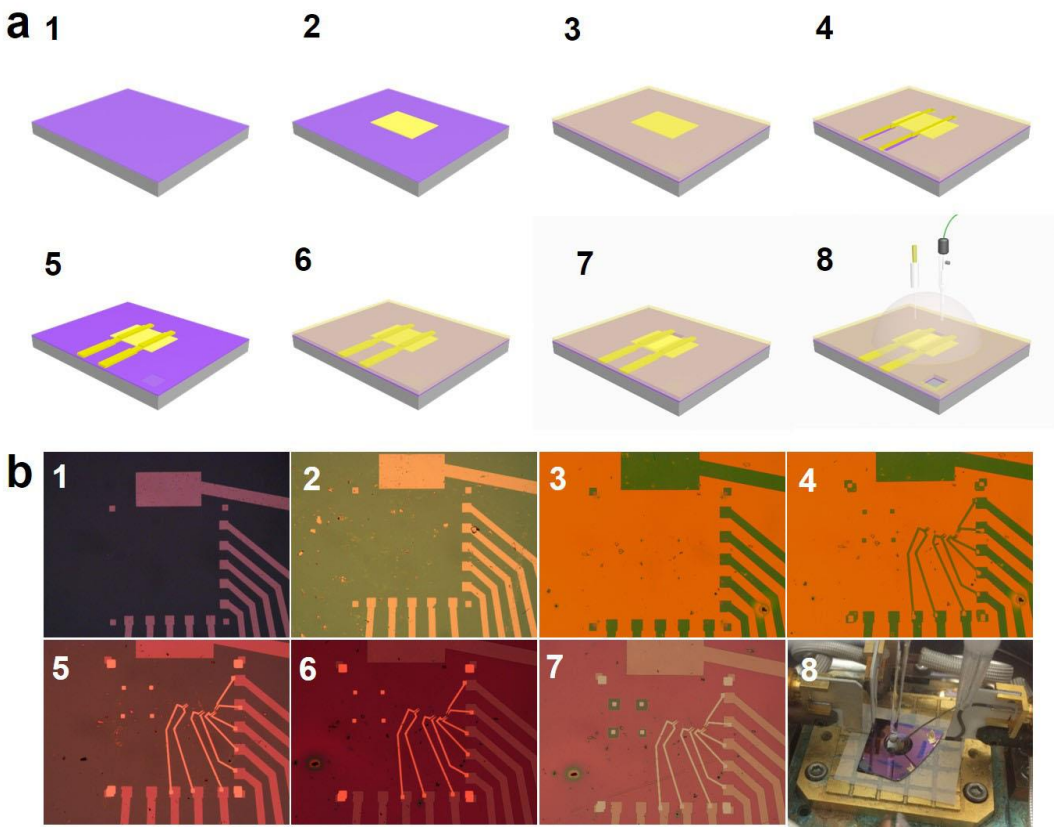

Figure S3. Fabrication process of the individual VSe_2 nanosheet based HER device. (a) The schematic of the fabrication process. (b) The optical micrograph of the fabrication process.

This process includes the following steps. Step 1, preparing a clean silicon wafer (with 300 nm SiO_2) with pre-patterned outer microelectrodes and positioning marks (Au/Cr, 50 nm/5 nm). Step 2, transferring VSe_2 nanosheets onto the silicon wafer with the assistant of tape. Step 3, MMA (methyl methacrylate, EL9, Microchem corp.) and PMMA (polymethyl methacrylate, A4, Microchem corp.) photoresists are spin-coated on the wafers (4000 rpm, bake at 180 ℃, 5 min). Step 4, patterning the metal contacts pad (inner microelectrodes) by e-beam lithography (EBL) on silicon wafers. Step 5, developing (mixed solution of methyl isobutyl ketone and isopropanol) and rinsing to remove the photoresists on the specific sites. Then, depositing 5 nm Cr (0.4 Å s^{-1}) and 150 nm Au (4 Å s^{-1}) on the wafers with

thermal evaporation under high vacuum condition and then lift off the extra gold on photoresists within N, N-Dimethylformamide. Step 6, spin-coating PMMA (3000 rpm, 2 layers, bake at 180 ℃, 5 min) on silicon wafers. Step 7, patterning with EBL to open a confined window which exposures the VSe_2 nanosheet and ensure the insulation of micro electrodes. Step 8, injecting 0.5 M H_2SO_4 on the surface of silicon wafer (keeps nanosheet immersed in electrolyte) and measuring data in probe station.

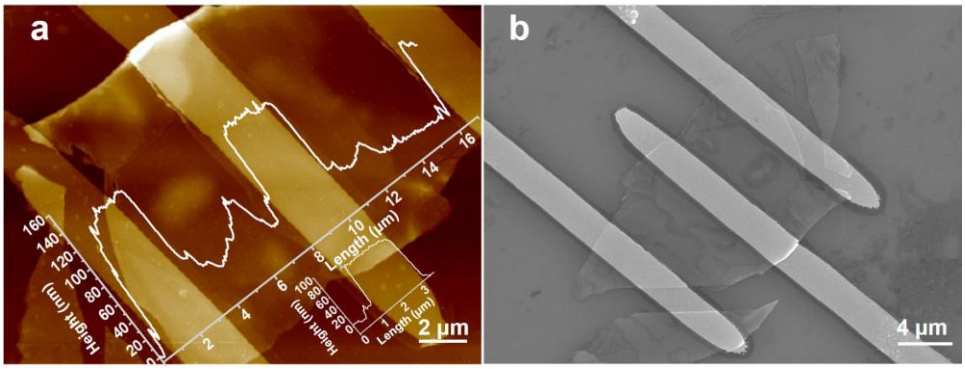

Figure S4. The atomic force microscopy image (a) and the corresponding SEM image (b) of an individual VSe_2 nanosheet which connects to three Cr/Au microelectrodes.

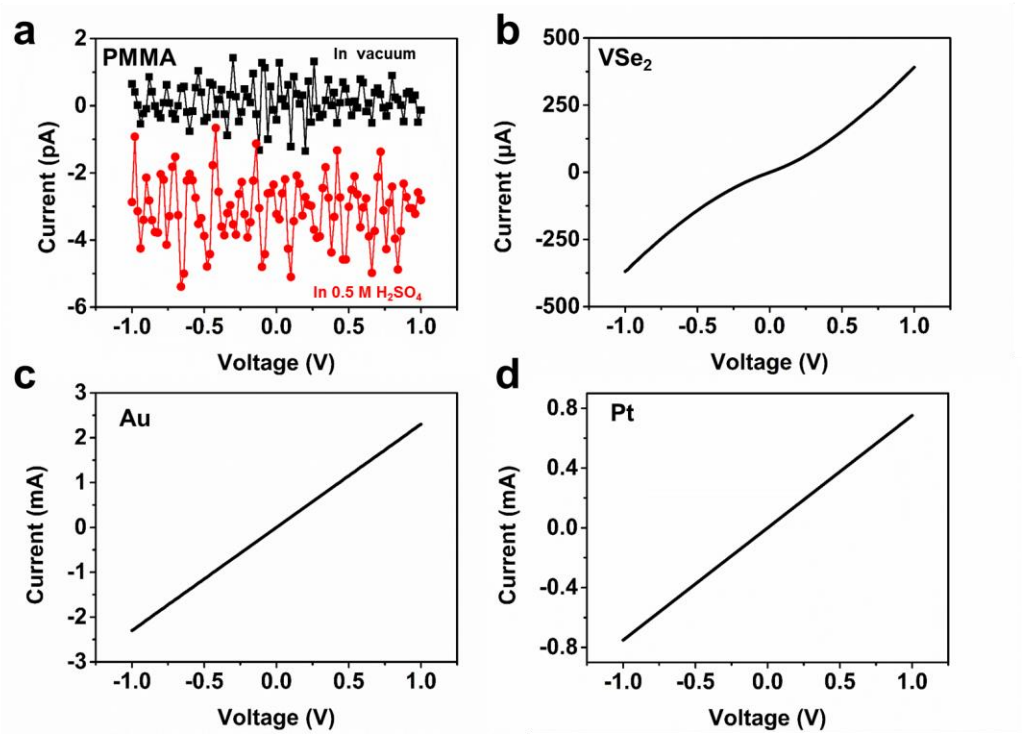

Figure S5. I-V plots of different samples. (a) PMMA (the black curve is in vacuum and the red one is in 0.5 M H_2SO_4), (b) VSe_2 nanosheet, (c) Au and (d) Pt. These measurements were conducted in vacuum by probe station combined with semiconductor device analyzer.

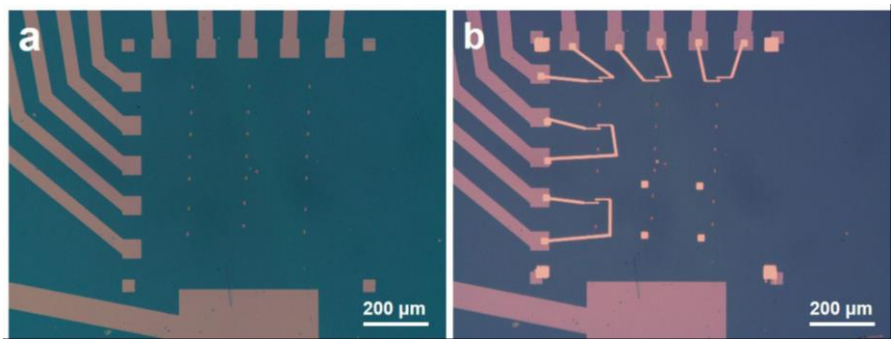

Figure S6. Optical micrograph of typical device fabrication process for the HER measurement of Pt. The fabrication process includes the following steps. Step 1, opening windows by EBL after coating PMMA on Si/SiO_2 wafer and then develop and rinse. Step 2, spurting Pt onto the wafer by Auto-fine Coater (JFC-1600). Step 3, patterning the metal contact pads with EBL on silicon wafers and then depositing 5

nm Cr and 150 nm Au on the wafer with thermal evaporation after developing and rinsing. Step 4, lift-off. Step 5, patterning with EBL to open a window which exposures the Pt after coating PMMA on silicon wafers. (a) Optical micrograph of the sample wafer after spurting Pt (~30 nm). (b) Optical micrograph of a silicon wafer after patterning the inner microelectrodes which connect the Pt to outer gold contact pads.

Conversion of potential from SCE to RHE

$E_{RHE}=E_{SCE}$ + 0.241 V + 0.059 V * pH. The electrolyte is 0.5 M H_2SO_4 and pH is 0. When measuring in 0.5 M H_2SO_4, $E_{RHE}=E_{SCE}$ + 0.241 V (298 K).

Current density calculation

Due to the convenience of individual nanosheet devices, we can calculate the exposed area of nanosheets. The exposure area is decided by the windows opened in PMMA insulator layer by EBL. In our devices, the area of individual nanosheet ranges from ~10 to ~40 μm^2. Meanwhile, the catalytic current can reaches 10^{-7} A. And such calculation will caused much higher current density than normal literature[1]. The polarization curve and Tafel plot before correction is shown in Figure S7a and b. Although this method of calculation is reliable, we use exchanges current density to correct the current density. Firstly, the same devices of gold (Au) and platinum (Pt) is fabricated. Details is shown in Figure S6, and the Au devices are fabricated the same way as Pt. The polarization curves are shown in Figure 2a and Tafel plot is shown in Figure S7c. The exchange current density (j_0) is calculated by the extrapolation of Tafel plots and the intercept of current density at overpotential (η) = 0 V is used as j_0. Based on the curves before correction, the j_0 of Au and Pt are $10^{-1.37}$ and $10^{-1.68}$ mA cm^{-2}, respectively. Although the values of j_0 differs a lot in different literature, the order of magnitude is usually the same.

Based on the data from literature, the $j_{0,Au}$ is ~10^{-3} mA cm^{-2} and $j_{0,Pt}$ is ~1 mA cm^{-2}. The difference between calculated values and standard values is both ~$10^{-1.66}$ mA cm^{-2} for Au and Pt. Based on this results, an exact methods for correction is shown as,

$$i_c = i_0 * \frac{\frac{j^S_{0,Pt}}{j_{0,Pt}} + \frac{j^S_{0,Au}}{j_{0,Au}}}{2},$$

where i_c and i_0 are the current density after correction and before, respectively, j_o^S is the standard exchange current density, j_o is the calculated exchange current density before correction. The Tafel plot after correction is shown in Figure S7d. Here, the iR correction is not calculated as the reference electrode is closed to the working electrode and the R_s (solution resistance) is low (~4.5 kΩ, calculated form EIS results). The iR-drop is negligible when the catalytic current is smaller than 10^{-7} A.

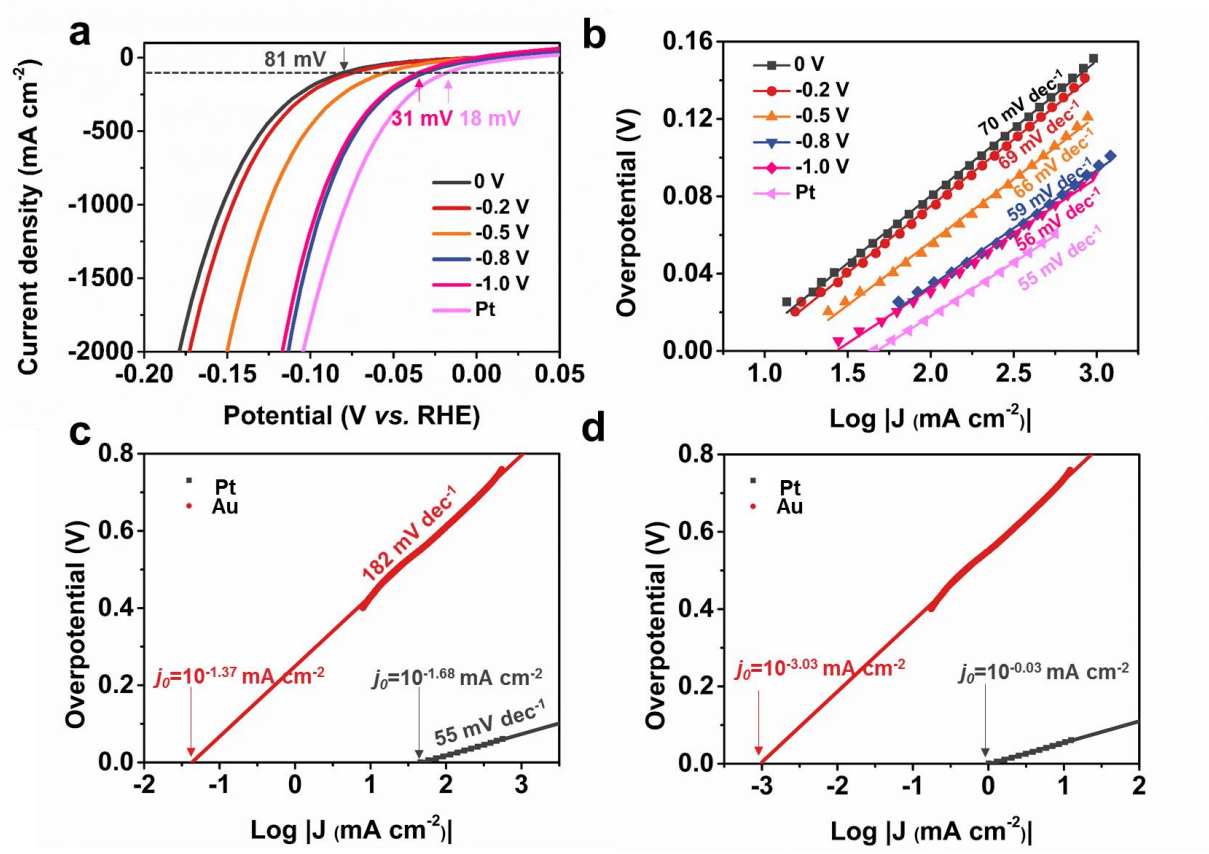

Figure S7. The HER performance of VSe_2 nanosheet and Tafel plots of Pt and Au. (a, b) The polarization curve and the corresponding Tafel plot of VSe_2 nanosheet. The current density is calculated from the real area. (c, d) The Tafel plots of Au and Pt and the calculated exchange current density before and after correction.

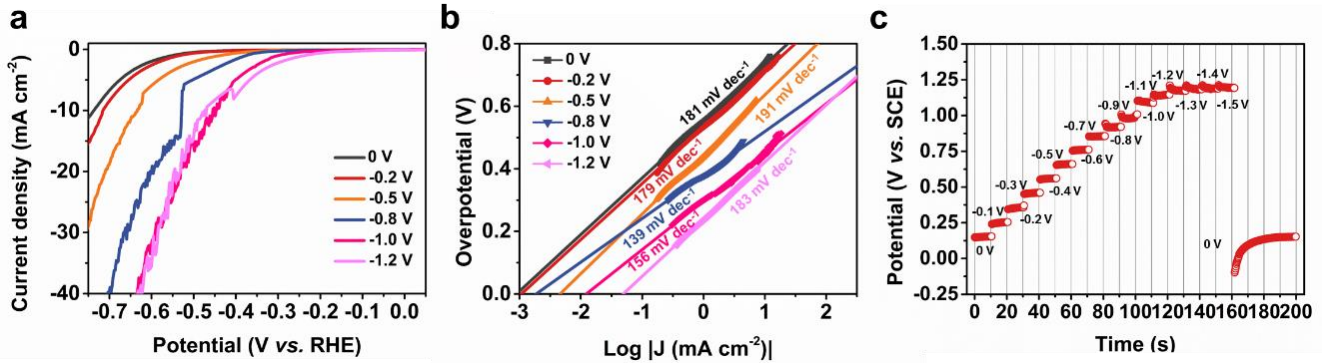

Figure S8. The HER performance of Au. (a, b) The polarization curve and Tafel plot of Au samples. (c) Gate-dependent open circuit potential of Au in 0.5 M H_2SO_4. Each step is -0.1 V and it holds for 10 s.

Turnover frequency (TOF) calculation

The turnover frequency value is calculated according to this equation[2].

$$\mathrm{TOF} = \frac{\text{Total number of } H_2 \text{ atoms per second}}{\text{Total number of active sites per unit area}} = \frac{j}{2qN}$$

Where j is current density (A cm^{-2}), number 2 means 2 electrons per H_2 molecule, q is the elementary charge which is 1.6×10^{-19} C and N is active site density (cm^{-2}). To calculate the TOF value, it is necessary to identify the active site density (N). In this work, we assumed that all the surface V atoms are the active sites because it is very difficult to identify the concentration of the Se vacancies. When we

calculate the TOF value by the area of the surface, we can obtain a limit value which is accurate to some degree[3]. Assuming a lattice constant of 3.36 Å, the surface of the unit cell will be 9.78×10^{-16} cm^2, $N \approx 1.33/ (9.78\times10^{-16}) = 1.36\times10^{15}$ cm^{-2}.

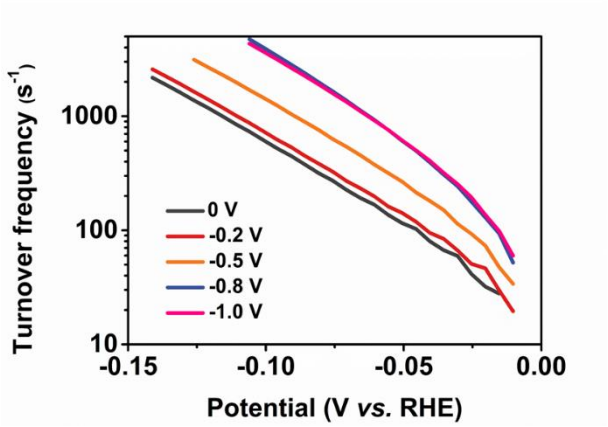

Figure S9. Turnover frequency per surface V atom calculated from corresponding polarization curves in Figure 2b.

Electrochemical impedance spectroscopy (EIS)

In this work, EIS was applied to investigate the electrochemical process at the interface between electrode and electrolyte. In a typical measurement, the frequency ranges from 10 kHz to 1 Hz. We didn't retain the data from 1 to 0.01 Hz because it is unwound and will cause much error when fitting the curves. The DC potential is set at -0.4 V *vs.* RHE.

When fitting the Nyquist plot, we use a typical two-time constant model[4]. The equivalent circuit is shown in Figure S10a. The CPE_1 and R_1 belong to the high frequency region and CPE_2 and R_2 belong to the low frequency region. The constant phase element (CPE) is described by:

$$Z_{CPE} = \frac{1}{Q(i\omega)^{\varphi}}$$

where Q is the capacity parameter, i = √-1, ω is the angular frequency of the AC voltage and φ ($0 < \varphi < 1$) is a dimensionless parameter related to the constant phase angle.

In this circuit, R_s is the resistance attributed to the uncompensated solution resistance, the high frequency time constant is related to the charge transfer process, R_1 (Faradaic resistance for the electrosorption, R_{ct}), CPE_1 (double layer capacitance, C_{dl}) and the low frequency time constant is related to the electrodesorption and/or recombination process, R_2 (Faradaic resistance for the electrodesorption and/or recombination reactions, R_p), CPE_2 (adsorption pseudocapacitance, C_p)[5].

The time constant (τ) value is calculated by:

$$\tau_i = \frac{1}{\omega^*} = R_i Q_i$$

where ω^* is characteristic angular frequency.

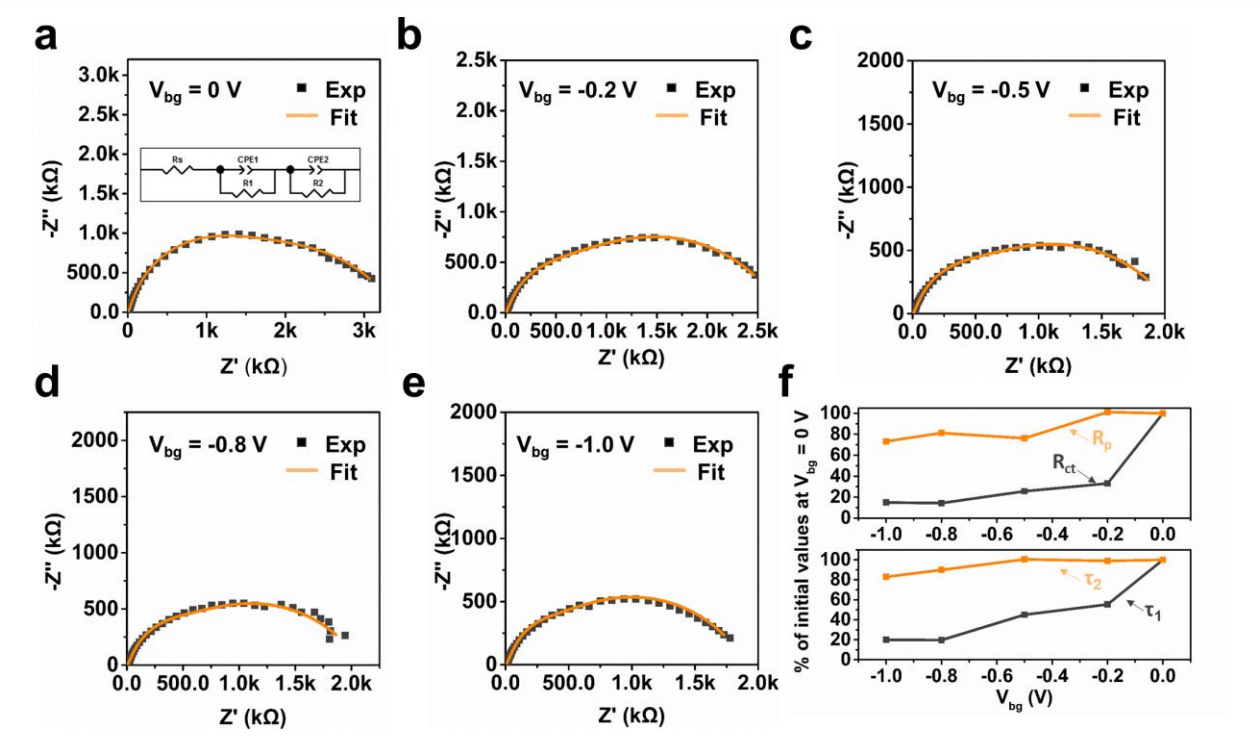

Figure S10. Nyquist plots from different negative back gate voltage. (a) V_{bg} = 0 V, inset is the fitting circuit. (b) V_{bg} = -0.2 V, (c) V_{bg} = -0.5 V, (d) V_{bg} = -0.8 V, (e) V_{bg} = -1 V and (f) the percentage change of relevant parameter. (The dots are the experiment data and the line represents the fitting result.)

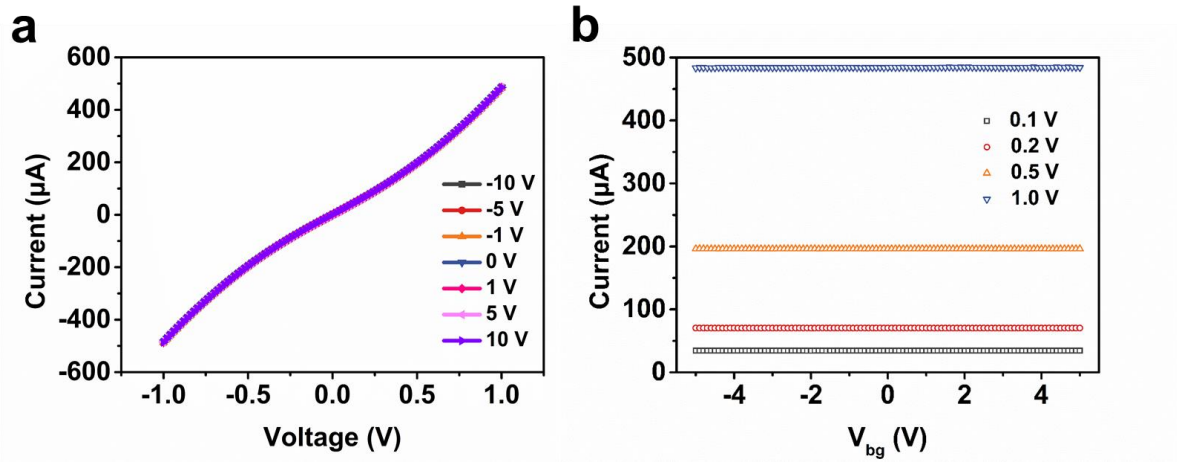

Figure S11. Plot of electrical properties measured from a typical VSe_2 nanosheet. (a) I_{ds}-V_{ds} plot of VSe_2 at different V_{bg} due to the metallic properties of VSe_2 nanosheet, these curves is coincident. (b) I_{ds}- V_{bg} plot of VSe_2 at different V_{ds}.

Continuum simulation

Here the continuum simulation was carried out using the COMSOL Multiphysics software to calculate the ion concentration in electrolyte under different additional back voltages. According to experimental system design, the micro-device structure could be simplified as a combination of 2D model with silicon dioxide (SiO_2), PMMA, active materials (VSe_2 nanosheet) and electrolyte (H_2SO_4). The dimension of structures of each component in the model was shown in Figure S12. The thickness of silicon dioxide, PMMA, and electrolyte were 300, 200, 400 nm respectively. One VSe_2 nanosheet (40 × 20 nm) was placed above the SiO_2 layer.

Based on the proposed 2D model, the biased electric potential difference ($\Delta\Phi$ = 0, -0.1V, -0.2V, -0.3V, -0.8V) was applied on the left (Γ_2) and right (Γ_1) end boundaries. This is to investigate the relation between the ions distribution and additional back gate voltage. Different material permittivity was employed for silicon dioxide (3.9)[6], VSe_2 nanosheets (10^{10}), PMMA (3.49)[7] and electrolyte (100)[8] respectively. The VSe_2 is the metal and its permittivity should be infinite. Here we choose 10^{10} as the value of its permittivity and we find that this value is valid since when increasing the value furthermore (to 10^{15}), negligible difference showed in results between 10^{10} and 10^{15}. On the boundary of (Γ_1), the constant H_2SO_4 concentration (0.5 M) was maintained to mimic the bulk electrolyte reservoir in the experiment. For the rest boundaries (Γ_3, Γ_4, Γ_5, Γ_6, Γ_7, Γ_8), the impermeable boundaries for both electric potential and concentration field were used.

The evolution of the 2D model was governed by the classic Poisson-Nernst-Planck (PNP) equation, which has been widely employed to describe the electrical double layer and nanofluidics devices. For the implemental detail, see our previous work for ion transport in graphene membrane[9]. The diffusion coefficient of H^+ ions was 9.31×10^{-5} cm^2/s and the figure for SO_4^{2-} was 1.06×10^{-5} cm^2/s[10] and the electric mobility of ion was derived from the Nernst-Einstein relation.

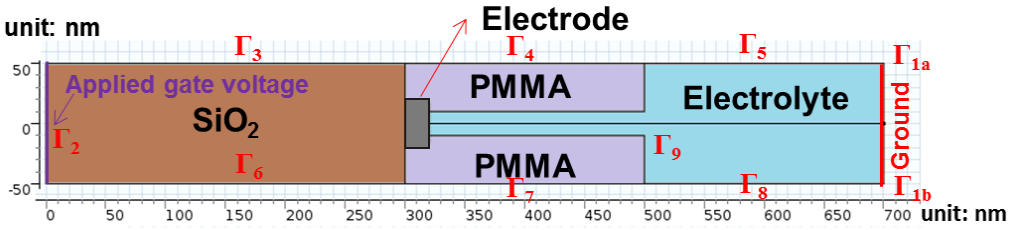

Figure S12. The schematic of COMSOL model. The brown, grey, and blue region represented the SiO_2, VSe_2 nanosheet and electrolyte, respectively. Note that Γ_9 was added as an assistant line for the post-analysis.

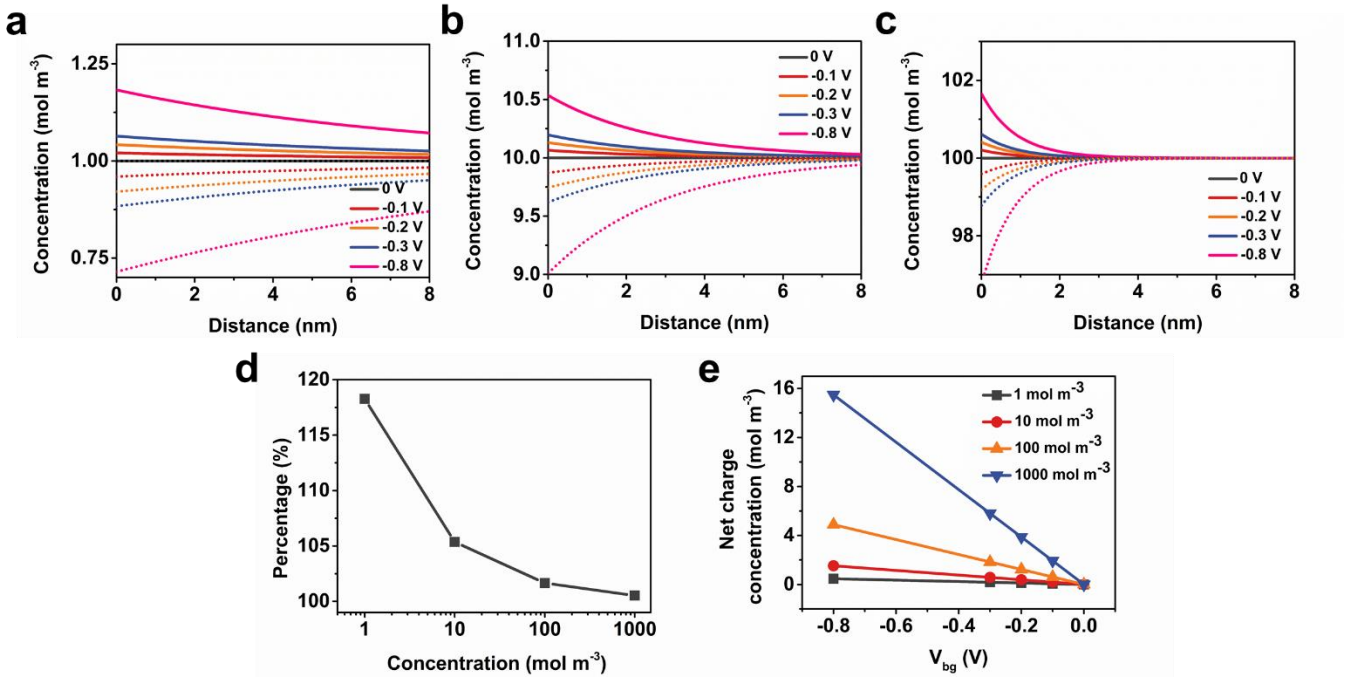

Figure S13. The computed concentration distribution of positive and negative charge (line represent H^+ and dots represent SO_4^{2-}, respectively) under different back gate voltages. (a-c) are concentration distributions of different initial concentration (1, 10, 100 mol m^{-3}). (d) The ratio of maximum concentration (V_{bg} = -0.8 V) and initial concentration of H^+. (e) The maximum net charge concentration at different back gate voltages. The net charge concentration is the difference value between negative and positive charge.

Reference

(1) Zhao, W.; Dong, B.; Guo, Z.; Su, G.; Gao, R.; Wang, W.; Cao, L. *Chem. Commun.* **2016,** 52, 9228-9231. doi:10.1039/C6CC03854A.

(2) Li, H.; Tsai, C.; Koh, A. L.; Cai, L.; Contryman, A. W.; Fragapane, A. H.; Zhao, J.; Han, H. S.; Manoharan, H. C.; Abild-Pedersen, F.; Norskov, J. K.; Zheng, X. *Nat. Mater.* **2015,** 15, 48-53. doi:10.1038/nmat4465.

(3) Voiry, D.; Fullon, R.; Yang, J.; de Carvalho Castro, E. S. C.; Kappera, R.; Bozkurt, I.; Kaplan, D.; Lagos, M. J.; Batson, P. E.; Gupta, G.; Mohite, A. D.; Dong, L.; Er, D.; Shenoy, V. B.; Asefa, T.; Chhowalla, M. *Nat. Mater.* **2016**. doi:10.1038/nmat4660.

(4) Kibsgaard, J.; Jaramillo, T. F.; Besenbacher, F. *Nat. Chem.* **2014,** 6, 248-53. doi:10.1038/nchem.1853.

(5) Azizi, O.; Jafarian, M.; Gobal, F.; Heli, H.; Mahjani, M. G. *Int. J. Hydrogen Energy* **2007,** 32, 1755-1761. doi:10.1016/j.ijhydene.2006.08.043.

(6) Gray, P. R.; Hurst, P. J.; Meyer, R. G.; Lewis, S. H., *Analysis and design of analog integrated circuits*. John Wiley & Sons, **2008**.

(7) Xie, L.; Huang, X.; Wu, C.; Jiang, P. *J. Mater. Chem.* **2011,** 21, 5897-5906. doi:10.1039/C0JM04574H.

(8) Greenwood, N. N.; Earnshaw, A. *Chemistry of the Elements*, Pergamon Press, **1984**.

(9) Cheng, C.; Jiang, G.; Garvey, C. J.; Wang, Y.; Simon, G. P.; Liu, J. Z.; Li, D. *Sci. Adv.* **2016,** 2, e1501272. doi:10.1126/sciadv.1501272.

(10) Cussler, E. L., *Diffusion: mass transfer in fluid systems*. Cambridge university press, **2009**.